Complex network analysis of resting-state fMRI of the brain*

Abdul Rauf Anwar[1*], Muhammad Yousaf Hashmy [2], Bilal Imran[2], Muhammad Hussnain Riaz[2], Sabtain Muhammad Muntazir Mehdi[2], Makii Muthalib[3], Stephane Perrey[3] Günther Deuschl[4], Sergiu Groppa[5], and Muthuraman Muthuraman[5]

***Abstract*— Due to the fact that the brain activity hardly ever diminishes in healthy individuals, analysis of resting state functionality of the brain seems pertinent. Various resting state networks are active inside the idle brain at any time. Based on various neuro-imaging studies, it is understood that various structurally distant regions of the brain could be functionally connected. Regions of the brain, that are functionally connected, during rest constitutes to the resting state network. In the present study, we employed the complex network measures to estimate the presence of community structures within a network. Such estimate is named as modularity. Instead of using a traditional correlation matrix, we used a coherence matrix taken from the causality measure between different nodes. Our results show that in prolonged resting state the modularity starts to decrease. This decrease was observed in all the resting state networks and on both sides of the brain. Our study highlights the usage of coherence matrix instead of correlation matrix for complex network analysis.**

I. INTRODUCTION

Recent research has shown that the brain activity exhibits impulsive changes in blood oxygen level-dependent (BOLD) signal. The BOLD signal is an indirect measure of the action potentials and neuronal activity of the brain. Hence, functional magnetic resonance imaging (fMRI) can help us to understand the functional working of the brain, particularly during the resting state [1]. The resting state is the state of brain when it is not subjected to carry out an evoked task. Since the extent of neuronal activity only changes marginally between the resting and activity states, analysis of neuronal activity during resting state is important [2]. The default mode network (DMN) gets activated instead of the task positive network (TPN) during resting state. The DMN is comprised of several different regions in the brain. In addition to DMN other networks also get activated, e.g., attention and auditory networks. The resting state networks are associated with low frequency fluctuations (LFF) of BOLD signal (0.01-0.1 Hz), hence the analysis of resting state networks in LFF frequency range seems promising [3]. Correlation provides the basis of understanding the functional segregation of the brain. If two regions of the brain show high correlation then both of them account for the same functional network inside the brain. The positive and negative values of correlation between two signals quantify if they are contributing in similar or dissimilar manner. Furthermore, the maximum value of correlation can also help to understand if one signal is delayed or advanced with respect to another one [4]. Despite being one of the foremost tools for analyzing the similarity between two signals (regions), correlation does not shed any light on the causality, i.e., direction of information flow between two signals. Such directionality can expose the inherent chronological time ordering of the signals. The direction of information between multiple signals can only be inferred by employing causality estimating measures on the signals of interest [4].

The classical methods of causality estimation for fMRI signals include structural equation modeling (SEM) and dynamic causal modeling (DCM). These methods rely on some a-priori assumption about underlying anatomical network, hence limiting interpretation of their results [5]. Another class of methods, known as parametric methods, is based on the idea that the subjected time series follows a linear regression and their regression coefficients can be exploited to quantify causality between them [6]. Parametric methods include methods like partial directed coherence (PDC) and directed transfer function (DTF). Further detail about parametric methods of causality estimation can be found elsewhere [4] [7].

Complex network analysis is another approach of understanding the functionally associated regions of the brain. It offers conveniences such as meaningful and easily measurable parameters to assess the degree of organization between different functionally connected regions of the brain [8]. In complex network analysis, we calculate various parameters to understand the relations and partitions present within the network. Further explanation about network analysis and various network parameters can be found elsewhere [8] [9]. Modularity is one network parameter, which quantifies the degree of different community structures within a network [10]. Furthermore, modularity has been reported to be of great significance in the assessment of time-varying attributes of functional brain connectivity [11]. There is a growing acceptance of the fact that most biological networks have a high degree of modularity within them, hence analyzing

[1]A. R. Anwar* is with Faculty of Biomedical Engineering Center, University of Engineering and Technology, Lahore (KSK), Pakistan. raufanwar at uet.edu.pk

[2]M. Y. Hashmy, B. Imran, M. H. Riaz and S. M. M. Mehdi are with Department of Electrical Engineering, University of Engineering and Technology, Lahore, Pakistan.

[3]M. Muthalib and S. Perrey are with Movement to Health (M2H), Euromov, Montpellier-1 University, Montpellier, France. makii.muthalib at univ-montp1.fr stephane.perrey at univ-montp1.fr

[4]G. Deuschl is with the Department of Neurology, Universitätsklinikum Schleswig-Holstein, Kiel, Germany. g.deuschl at neurologie.uni-kiel.de

[5]S. Groppa and M. Muthuraman are with the Department of Neurology, University of Mainz, Mainz, Germany. segroppa at uni-mainz.de mmuthura at uni-mainz.de

the modularity between different brain networks seems pragmatic [12].

II. METHODS

The parametric methods of causality estimation can only be applied to the stationary signals, however, in reality most of the physiological signals are non-stationary in nature [8]. This can better be explained by considering a general expression of auto-regressive (AR) model with order p as [13]

$$y_i(t) = \sum_{r=1}^{r=p} a_{ij,r} y_j(t-r) + \eta(t). \quad (1)$$

In Equation 1, $\eta(t)$ is the random white noise while $a_{ij,r}$ are the multivariate auto-regressive coefficients (MVAR), describing the effect of time series y_j on time series y_i corresponding to delay r. The model order p specifies the memory of the model, i.e., how many past values of y_j are required to completely describe its influence on y_i. In case of non-stationary signals, Equation 1 becomes [13]

$$y_i(t) = \sum_{r=1}^{r=p} a_{ij,r}(t) y_j(t-r) + \eta(t). \quad (2)$$

As we can see that in Equation 2, MVAR coefficients have now become time-dependent $a_{ij,r}(t)$, hence now accommodating the non-stationarity of the signals. The estimation of these time-varying coefficients is complicated. However, it can be solved using the dual extended Kalman filters (DEKF) to calculate them [12]. The details about the usage of DEKF to calculate time-varying MVAR coefficients can be found elsewhere [14]. After the estimation of these parameters, a variant of PDC known as time-resolved partial directed coherence (tPDC) is used to quantify the causality from one signal to another signal. The expression of tPDC, based on the original expression of PDC [15], can be given as

$$|\pi_{i \leftarrow j}(\omega, t)| = \frac{|A_{ij}(\omega, t)|}{\sqrt{\sum_k |A_{kj}(\omega, t)|^2}}. \quad (3)$$

In the above expression, the term $\pi_{i \leftarrow j}(\omega, t)$ expresses the absolute magnitude of causality, in terms of coherence, normalized to be between zero and one. The term $A_{ij}(\omega, t)$ is the Fourier transform of $a_{ij,r}(t)$, already defined in Equation 2. Mathematically, $\pi_{i \leftarrow j}(\omega, t)$ is a matrix with scalar coherence values stored inside. On one axis there is a frequency range, while the other axis gives a complete time range, hence using tPDC we can target any frequency and time of our interest, while analyzing the causality between signals. In the current study, we used tPDC to focus on LFF frequency range and derived a directed coherence matrix based on causality magnitudes. The resulting matrix can then be used to estimate the network attributes by estimating modularity. The mathematical expression of modularity can be given as [8] [16]

$$Q = \sum_{u \in M} \left[e_{uu} - \left(\sum_{v \in M} e_{vu} \right)^2 \right], \quad (4)$$

where M is the number of distinct modules into which the network is partitioned. The proportion of all the links that join nodes in module u with nodes in module v [8]. The modularity Q is a scalar measure, having either a positive or a negative value. The positive modularity indicates the presence of community structure within a network [10].

III. DATA ACQUISITION

In the present study, the resting state fMRI was recorded from eleven healthy subjects (mean age 25 years, seven females) for 10 minutes. BOLD-sensitive MRI was performed with a 3-Tesla MR scanner (Philips, the Netherlands). A single-shot T1-weighted, gradient-echo planar imaging sequence was used for fMRI (TR = 2500 ms, TE = 45 ms, 32 slices, 64 x 64 matrix, slice thickness = 3.5 mm, FOV = 200 mm, flip angle = 90). With a repetition time of 2.5 seconds, 240 fMRI volumes were acquired in 600 seconds. A written consent was taken from all the subjects and experiment was carried out in compliance with Helsinki declaration.

Afterwards, all volumes were realigned to mitigate the movement-related artifacts. Realignment was followed by normalization, smoothing and slice time correction. The first 10 fMRI volumes were disposed off in order to lessen the contributions of initial noise and magnetic saturation effects. Using automated anatomical labeling (AAL), the brain was parcellated into 116 regions and time course from each region was extracted using toolboxes named CONN15 and SPM08 (http://www.fil.ion.ucl.ac.uk/spm) [17] [18] [19]. Out of those 116 regions of the brain, 45 were chosen on the basis of their involvement in resting state networks. The details of these regions and corresponding networks are highlighted in Table I and II [20].

By choosing an optimum model order, the tPDC was applied to fMRI time courses within each network in the both hemispheres. Since, fMRI was recorded at a sampling rate of 0.4 Hz, we can resolve till the frequency of 0.2 Hz on the frequency axis of tPDC matrix. Since we are interested in only low frequency fluctuations (LFF), the portion of tPDC matrix corresponding to 0.01-0.1 Hz was taken. Then the whole time axis of tPDC matrix was divided into eight windows and the data within each window was averaged to a yield single value for each window. Finally, a coherence matrix was constructed between all the nodes of each network based on the magnitudes of tPDC. This coherence matrix has an intrinsic directed information and hence can be used to analyze the complex network parameters for each resting state network. This matrix was fed to the Brain Connectivity Toolbox (BCT) and modularity was estimated for each resting state network and for each time window.

IV. RESULTS

The results of this analysis are shown in Figures 1 and 2. We can observe that the typical modularity values for all RSNs lie within range of 0.3 to 0.4. Furthermore, over the course of time we can see that the values of modularity decrease for all RSNs on both the hemispheres of the brain. Since the difference in amplitudes between successive

TABLE I

NAMES AND ABBREVIATIONS OF DIFFERENT BRAIN REGIONS WHICH CONSTITUTE TO RESTING STATE NETWORKS. EACH NODE IS PRESENT IN BOTH HEMISPHERES [20].

Regions	Abbreviation	Regions	Abbreviation
Amygdala	AMYG	Orbitofrontal cortex (middle)	ORBmid
Angular gyrus	ANG	Orbitofrontal cortex (superior)	ORBsup
Anterior Cingulate gyrus	ACG	Pallidum	PAL
Calcarine cortex	CAL	Paracentral Lobule	PCL
Caudate	CAU	Parahippocampal gyrus	PHG
Cuneus	CUN	Postcentral gyrus	PoCG
Fusiform gyrus	FFG	Posterior cingulate gyrus	PCG
Heschl gyrus	HES	Precentral gyrus	PreCG
Hippocampus	HIP	Precuneus	PCUN
Inferior ocipital gyrus	IOG	Putamen	PUT
Inferior frontal gyrus (opercula)	IFGoperc	Rectus gyrus	REC
Inferior frontal gyrus (triangular)	IFGtriang	Rolandic operculum	ROL
Inferior parietal lobule	IPL	Superior occipital gyrus	SOG
Inferior temporal gyrus	ITG	Superior frontal gyrus (dorsal)	SFGdor
Insula	INS	Superior frontal gyrus (medial)	SFGmed
Lingual gyrus	LING	Superior parietal gyrus	SPG
Middle cingulate gyrus	MCG	Superior temporal gyrus	STG
Middle occipital gyrus	MOG	Supplementary motor area	SMA
Middle frontal gyrus	MFG	Supramarginal gyrus	SMG
Middle temporal gyrus	MTG	Temporal pole (middle)	TPOmid
Olfactory temporal gyrus	OLF	Temporal pole (superior)	TPOsup
Orbitofrontal cortex (inferior)	ORBinf	Thalamus	THA
Orbitofrontal cortex (medial)	ORBmed		

windows is very small, we only performed the t-test between first and last window. The results of the t-test show that there is a significant ($p < 0.05$) decrease in the last window as compared to the first window, except for RSN4 on right side. The results of the t-test analysis between the first and last windows is shown in Table III and Table IV.

V. CONCLUSIONS

In the presented work, we applied complex network analysis measures on the tPDC generated coherence matrices to examine the changes in network traits over the course

TABLE II

DETAILS ABOUT COMPOSITION OF DIFFERENT RESTING STATE NETWORKS. NAMES OF NODES ARE GIVEN IN ABBREVIATED FORM. FOR FULL NAMES PLEASE REFER TO TABLE I [20].

	Network	Regions Involved
RSN1	Default Mode Network	ORBmed, SFGdor, PCUN, MTG, TPOmid, ACG, ANG, REC, PCG, SFGmed
RSN2	Attention Network	IFGtriang, ORBmid, IPL, IFGoperc, SPG, ORBsup, MFG, ORBinf
RSN3	Visual Recognition Network	LING, IOG, FFG, CUN, CAL, SOG, MOG
RSN4	Auditory Network	SMG, ROL, HES, INS, TPOsup, STG
RSN5	Sensory-motor Network	PCL, PoCG, SMA, PreCG
RSN6	Sub-cortical Network	OLF, THA, PUT, HIP, CAU, AMYG, MCG, ITG, PHG, PAL

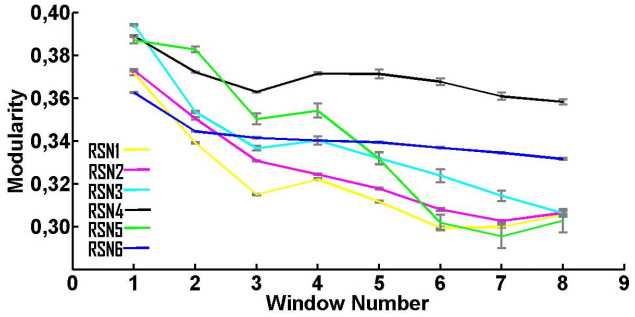

Fig. 1. Results of modularity between different windows on left side of the brain. A clear downward trend among all resting state networks is visible.

of time. We focused on modularity, since it helps us to quantify the segregation within the network by estimating the number of smaller communities. The presence of smaller communities in the brain network has long been established [21]. On the basis of our results, we can see that as the resting state goes on, the modularity within each RSN starts to reduce slightly. This implies that as the brain goes into an extended resting state, functional segregation of different sub-communities starts to cease. As per literature, a decrease in modularity was observed in the case of aging and disease [22] [23] [24]. Moreover, a change in modularity over the course of time during the resting state fMRI was also observed [25]. We speculate that as the brain steps into 'pre-sleep' mode, brain communities start to lose their distinctiveness. However, further studies need to be done in order to better understand the working of the brain during resting state.

REFERENCES

[1] H.Jahanian, W. W. Ni, T. Christen, M. E. Moseley, M. K. Tamura, G. Zaharchuk, "Spontaneous BOLD Signal Fluctuations in Young Healthy Subjects and Elderly Patients with Chronic Kidney Disease, Plos One, Volume 9, Issue 3, pp. e92539, 2014.

[2] A. R. Anwar; M. Muthalib; S. Perrey; S. Wolff; G. Deuschl; U. Heute; M. Muthuraman, "Differences in hemispherical thalamo-cortical causality analysis during resting-state fMRI," in Engineering

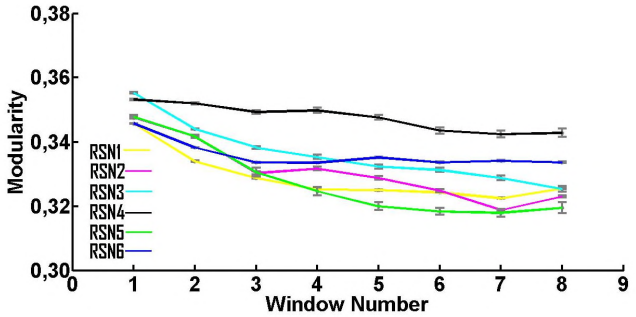

Fig. 2. Modularity results on right side of the brain show a downward trend among all RSNs. The RSN4 has higher modularity than other networks.

TABLE III

MEAN AND STANDARD DEVIATION OF MODULARITY AMONG 11 SUBJECTS IN FIRST AND LAST WINDOW ON LEFT SIDE OF THE BRAIN. RESULTS SHOW THAT DIFFERENCE BETWEEN TWO WINDOWS IN ALL NETWORKS IS SIGNIFICANT.

	Mean	Std. Deviation	p-value/pair
RSN1-Left-Window 1	0.3716	0.031	0.000
RSN1-Left-Window 8	0.3055	0.023	
RSN2-Left-Window 1	0.3729	0.026	0.000
RSN2-Left-Window 8	0.3064	0.031	
RSN3-Left-Window 1	0.3941	0.021	0.000
RSN3-Left-Window 8	0.3063	0.045	
RSN4-Left-Window 1	0.3891	0.019	0.011
RSN4-Left-Window 8	0.3582	0.036	
RSN5-Left-Window 1	0.3870	0.039	0.002
RSN5-Left-Window 8	0.3028	0.077	
RSN6-Left-Window 1	0.3716	0.031	0.000
RSN6-Left-Window 8	0.3035	0.023	

TABLE IV

MEAN AND STANDARD DEVIATION OF MODULARITY AMONG 11 SUBJECTS IN FIRST AND LAST WINDOW ON RIGHT SIDE OF THE BRAIN. DIFFERENCE BETWEEN FIRST AND LAST WINDOW IN RSN4 IS, HOWEVER, NOT SIGNIFICANT.

	Mean	Std. Deviation	p-value/pair
RSN1-Left-Window 1	0.3642	0.018	0.000
RSN1-Left-Window 8	0.3137	0.024	
RSN2-Left-Window 1	0.3687	0.024	0.000
RSN2-Left-Window 8	0.3074	0.030	
RSN3-Left-Window 1	0.3881	0.027	0.000
RSN3-Left-Window 8	0.3134	0.049	
RSN4-Left-Window 1	0.3830	0.029	0.100
RSN4-Left-Window 8	0.3571	0.058	
RSN5-Left-Window 1	0.3695	0.040	0.003
RSN5-Left-Window 8	0.2987	0.067	
RSN6-Left-Window 1	0.3643	0.018	0.001
RSN6-Left-Window 8	0.3341	0.022	

in Medicine and Biology Society (EMBC), 2014 36th Annual International Conference of the IEEE , 26-30 Aug, pp. 990-993, 2014.

[3] P. Fransson, "Spontaneous low-frequency BOLD signal fluctuations: an fMRI investigation of the resting-state default mode of brain function hypothesis", Hum Brain Mapp., Sep 26, pp. 15-29. 2005.

[4] K. J. Blinowska. Review of the Methods of Determination of Directed Connectivity from Multichannel Data. Medical and Biological Engineering and Computing, volume 49, pp 521529, 2011.

[5] K. E. Stephen, K. j. Friston, "Analyzing effective connectivity with fMRI", Wiley Inter discip Rev Cogn Sci., vol. 1, no. 3, pp. 446-459, 2010.

[6] M. Jafari-Mamaghani, "Non-parametric analysis of Granger causality using local measures of divergence", Applied Mathematical Sciences, Vol. 7, no. 83, pp 4107-4136, 2013.

[7] M. Winterhalder, B. Schelter, W. Hesse, K. Schwab, L. Leistritz, D. Klan, R. Bauer, J. Timmer, H. Witte, "Comparison of linear signal processing techniques to infer directed interactions in multivariate neural systems", Signal Processing, Volume 85, Issue 11, pp. 2137-2160, 2005.

[8] M. Rubinov, O. Sporns, "Complex network measures of brain connectivity: Uses and interpretations", NeuroImage, Volume 52, pp. 10591069, 2010.

[9] M. E. J. Newman, "The Structure and Function of Complex Networks", SIAM Rev., Volume 45, Issue 2, pp. 167256, 2003.

[10] M. E. J. Newman, "Modularity and community structure in networks", PNAS, Volume 103, Issue 23, pp. 8577-8582, 2006.

[11] L. Ferrarini, I. M. Veer, E. Baerends, M. J. van Tol, R. J. Renken, N. J. van der Wee, D. J. Veltman, A. Aleman, F. G. Zitman, B. W. Penninx, M. A. van Buchem, J. H. Reiber, S. A. Rombouts, J. Milles, "Hierarchical functional modularity in the resting-state", Hum Brain Mapp., Jul 30, volume 7, pp. 2220-31, 2009.

[12] H-M. Kaltenbach, J. Stelling, "Modular Analysis of Biological Networks", Advances in Systems Biology, Volume 736, pp. 3-17, 2011.

[13] A. R. Anwar, K. G. Mideska, H. Hellriegel, N, Hoogenboom, H. Krause, A. Schnitzler, G. Deuschl, J. Raethjen, U. Heute, M. Muthuraman, "Multi-modal causality analysis of eyes-open and eyes-closed data from simultaneously recorded EEG and MEG," in Engineering in Medicine and Biology Society (EMBC), 36th Annual International Conference of the IEEE , vol., no., pp.2825-2828, 26-30 Aug, 2014.

[14] E. A. Wan, A. T. Nelson, "Kalman Filtering and Neural Networks", John Wiley and Sons, Inc., ch. 5., 2002.

[15] B. Schelter, L. Sommerlade, B. Platt, A. Plano, M. Thiel, J. Timmer, "Multivariate analysis of dynamical processes with applications to the neurosciences", Engineering in Medicine and Biology Society, EMBC, 2011 Annual International Conference of the IEEE, vol., no., pp.5931 - 5934, Aug. 30-Sept. 3, 2011.

[16] M. E. J. Newman, "Fast algorithm for detecting community structure in networks", Phys. Rev. E 69, 066133, 2004.

[17] S. Whitfield-Gabrieli, A. Nieto-Castanon, "Conn: A functional connectivity toolbox for correlated and anticorrelated brain networks". Brain Connectivity, volume 2, issue 3, pp. 125-41, 2012.

[18] X.J. Chai, A. Nieto-Castanon, D. Ongur, S. Whitfield-Gabrieli, "Anticorrelations in resting state networks without global signal regression". NeuroImage, volume 59, issue 2, pp. 1420-1428, 2012.

[19] N. Tzourio-Mazoyera, B. Landeaub, D. Papathanassioua, F. Crivelloa, O. Etarda, N. Delcroixa, B. Mazoyerc, M. Joliota, "Automated Anatomical Labeling of Activations in SPM Using a Macroscopic Anatomical Parcellation of the MNI MRI Single-Subject Brain", NeuroImage, volume 15, issue 1, pp. 273289, 2002.

[20] H. Tao, S. Guo, T. Ge, K. M. Kendrick, Z. Xue, Z. Liu and J. Feng, "Depression uncouples brain hate circuit", Molecular Psychiatry, volume 18, pp. 101111, 2013.

[21] J.D. Rudie, J.A. Brown, D. Beck-Pancer, L.M. Hernandez, E.L. Dennis, P.M. Thompson, S.Y. Bookheimer, M. Dapretto, "Altered functional and structural brain network organization in autism", NeuroImage: Clinical Volume 2, Pages 7994, 2013.

[22] A. F. Alexander-Bloch, N. Gogtay, D. Meunier, R. Birn, L. Clasen, F. Lalonde, R. Lenroot, J. Giedd and E. T. Bullmore, "Disrupted Modularity and Local Connectivity of Brain Functional Networks in Childhood-Onset Schizophrenia", Front Syst Neurosci., volume 4, issue 147, 2010.

[23] K. Onoda, S. Yamaguchi, "Small-worldness and modularity of the resting-state functional brain network decrease with aging", Neurosci Lett., volume 556, pp. 104-8., 2013.

[24] M. Caoa, J. H. Wang, Z. J. Daia, X. Y. Cao, L. L. Jiang, F. M. Fan, X. W. Song, M. R. Xia, N. Shu, Q. Dong, M. P. Milham, F. X. Castellanos, X. N. Zuo, Y. He, "Topological organization of the human brain functional connectome across the lifespan", Developmental Cognitive Neuroscience Volume 7, Pages 7693. 2014.

[25] R. F. Betzela, M, Fukushima, Y. He, X. N. Zuo, O. Sporns, "Dynamic fluctuations coincide with periods of high and low modularity in resting-state functional brain networks", NeuroImage, Volume 127, Pages 287297, 2016.